Research Article | Vol. 7, No. 9 | 1 Sep 2016 | BIOMEDICAL OPTICS EXPRESS 3574
Biomedical Optics EXPRESS

Direct visualization of functional heterogeneity in hepatobiliary metabolism using 6-CFDA as model compound

CHIH-JU LIN,[1] FENG-CHIEH LI,[1] YU-YANG LEE,[1] TE-YU TSENG,[1] WEI-LIANG CHEN,[1] VLADIMIR HOVHANNISYAN,[1] NING KANG,[1] NICHOLAS G. HORTON,[2] SHU-JEN CHIANG,[1] CHRIS XU,[2] HSUAN-SHU LEE,[3,4,7] AND CHEN-YUAN DONG[1,5,6,8]

[1]*Department of Physics, National Taiwan University, Taipei 106, Taiwan*
[2]*School of Applied and Engineering Physics, Cornell University, Ithaca, NY, 14853, USA*
[3]*Department of Internal Medicine, National Taiwan University Hospital and National Taiwan University College of Medicine, Taipei 100, Taiwan*
[4]*Institute of Biotechnology, National Taiwan University, Taipei 106, Taiwan*
[5]*Center for Optoelectronic Biomedicine, National Taiwan University, Taipei 106, Taiwan*
[6]*Center for Quantum Science and Engineering, National Taiwan University, Taipei 106, Taiwan*
[7]*benlee@ntu.edu.tw*
[8]*cydong@phys.ntu.edu.tw*

Abstract: Hepatobiliary metabolism is one of the major functions of the liver. However, little is known of the relationship between the physiological location of the hepatocytes and their metabolic potential. By the combination of time-lapse multiphoton microscopy and first order kinetic constant image analysis, the hepatocellular metabolic rate of the model compound 6-carboxyfluorescein diacetate (6-CFDA) is quantified at the single cell level. We found that the mouse liver can be divided into three zones, each with distinct metabolic rate constants. The sinusoidal uptake coefficients k_1 of Zones 1, 2, and 3 are respectively 0.239 ± 0.077, 0.295 ± 0.087, and 0.338 ± 0.133 min^{-1}, the apical excreting coefficients k_2 of Zones 1, 2, and 3 are 0.0117 ± 0.0052, 0.0175 ± 0.0052, and 0.0332 ± 0.0195 min^{-1}, respectively. Our results show not only the existence of heterogeneities in hepatobiliary metabolism, but they also show that Zone 3 is the main area of metabolism.

©2016 Optical Society of America

OCIS codes: (190.0190) Nonlinear optics; (190.4180) Multiphoton processes

References and links

1. K. Jungermann and T. Kietzmann, "Zonation of parenchymal and nonparenchymal metabolism in liver," Annu. Rev. Nutr. **16**(1), 179–203 (1996).
2. M. E. Brosnan and J. T. Brosnan, "Hepatic glutamate metabolism: a tale of 2 hepatocytes," Am. J. Clin. Nutr. **90**(1), 857S–861S (2009).
3. N. Katz and K. Jungermann, "Autoregulatory shift from fructolysis to lactate gluconeogenisis in rat hepatocyte suspensions. The problem of metabolic zonation of liver parenchyma," Hoppe Seylers Z. Physiol. Chem. **357**(3), 359–376 (1976).
4. J. W. Grisham, *Organizational principles of the liver.* (John Wiley & Sons, Ltd, 2009).
5. F. Kiernan, "The anatomy and physiology of the liver," Philos. Trans. R. Soc. Lond. **123**(0), 711–770 (1833).
6. A. M. Rappaport, Z. J. Borowy, W. M. Lougheed, and W. N. Lotto, "Subdivision of hexagonal liver lobules into a structural and functional unit; role in hepatic physiology and pathology," Anat. Rec. **119**(1), 11–33 (1954).
7. D. Ferri, L. Moro, M. Mastrodonato, F. Capuano, E. Marra, G. E. Liquori, and M. Greco, "Ultrastructural zonal heterogeneity of hepatocytes and mitochondria within the hepatic acinus during liver regeneration after partial hepatectomy," Biol. Cell **97**(4), 277–288 (2005).
8. R. Gebhardt, H. J. Burger, H. Heini, K. L. Schreiber, and D. Mecke, "Alterations of hepatic enzyme levels and of the acinar distribution of glutamine synthetase in response to experimental liver injury in the rat," Hepatology **8**(4), 822–830 (1988).
9. W. H. Lamers, A. Hilberts, E. Furt, J. Smith, G. N. Jonges, C. J. van Noorden, J. W. Janzen, R. Charles, and A. F. Moorman, "Hepatic enzymic zonation: a reevaluation of the concept of the liver acinus," Hepatology **10**(1), 72–76 (1989).

#264923 http://dx.doi.org/10.1364/BOE.7.003574
Journal © 2016 Received 10 May 2016; revised 2 Jul 2016; accepted 20 Jul 2016; published 19 Aug 2016

Biomedical Optics EXPRESS

10. E. Jigorel, M. Le Vee, C. Boursier-Neyret, Y. Parmentier, and O. Fardel, "Differential regulation of sinusoidal and canalicular hepatic drug transporter expression by xenobiotics activating drug-sensing receptors in primary human hepatocytes," Drug Metab. Dispos. **34**(10), 1756–1763 (2006).
11. I. Braakman, G. M. M. Groothuis, and D. K. F. Meijer, "Acinar redistribution and heterogeneity in transport of the organic cation rhodamine B in rat liver," Hepatology **7**(5), 849–855 (1987).
12. R. Gebhardt, A. Baldysiak-Figiel, V. Krügel, E. Ueberham, and F. Gaunitz, "Hepatocellular expression of glutamine synthetase: an indicator of morphogen actions as master regulators of zonation in adult liver," Prog. Histochem. Cytochem. **41**(4), 201–266 (2007).
13. C. Torre, C. Perret, and S. Colnot, "Transcription dynamics in a physiological process: β-catenin signaling directs liver metabolic zonation," Int. J. Biochem. Cell Biol. **43**(2), 271–278 (2011).
14. I. A. Sherman and M. M. Fisher, "Hepatic transport of fluorescent molecules: in vivo studies using intravital TV microscopy," Hepatology **6**(3), 444–449 (1986).
15. A. L. Dogan, O. Legrand, A. M. Faussat, J. Y. Perrot, and J. P. Marie, "Evaluation and comparison of MRP1 activity with three fluorescent dyes and three modulators in leukemic cell lines," Leuk. Res. **28**(6), 619–622 (2004).
16. P. Y. Wang, M. Boccanfuso, A. M. Lemay, H. Devries, J. Sui, Y. She, and C. E. Hill, "Sex-specific extraction of organic anions by the rat liver," Life Sci. **82**(7-8), 436–443 (2008).
17. K. S. Fenner, H. M. Jones, M. Ullah, S. Kempshall, M. Dickins, Y. Lai, P. Morgan, and H. A. Barton, "The evolution of the OATP hepatic uptake transport protein family in DMPK sciences: from obscure liver transporters to key determinants of hepatobiliary clearance," Xenobiotica **42**(1), 28–45 (2012).
18. D. M. van der Kolk, E. G. de Vries, J. A. Koning, E. van den Berg, M. Müller, and E. Vellenga, "Activity and expression of the multidrug resistance proteins MRP1 and MRP2 in acute myeloid leukemia cells, tumor cell lines, and normal hematopoietic CD34+ peripheral blood cells," Clin. Cancer Res. **4**(7), 1727–1736 (1998).
19. F. C. Li, Y. Liu, G.-T. Huang, L.-L. Chiou, J.-H. Liang, T.-L. Sun, C.-Y. Dong, and H.-S. Lee, "In vivo dynamic metabolic imaging of obstructive cholestasis in mice," Am. J. Physiol.-Gastroint. Liver Physiol. **296**(5), G1091–G1097 (2009).
20. Y. Liu, H. C. Chen, S. M. Yang, T. L. Sun, W. Lo, L. L. Chiou, G. T. Huang, C. Y. Dong, and H. S. Lee, "Visualization of hepatobiliary excretory function by intravital multiphoton microscopy," J. Biomed. Opt. **12**(1), 014014 (2007).
21. D. Keppler and I. M. Arias, "Hepatic canalicular membrane. Introduction: transport across the hepatocyte canalicular membrane," FASEB J. **11**(1), 15–18 (1997).
22. H. J. Varghese, L. T. MacKenzie, A. C. Groom, C. G. Ellis, A. F. Chambers, and I. C. MacDonald, "Mapping of the functional microcirculation in vital organs using contrast-enhanced in vivo video microscopy," Am. J. Physiol. Heart Circ. Physiol. **288**(1), H185–H193 (2004).
23. A. Takatori, M. Akahori, S. Kawamura, S. Itagaki, and Y. Yoshikawa, "Localization and age-related changes in cytochrome P450 expression in APA hamster livers," Exp. Anim. **49**(3), 197–203 (2000).

1. Introduction

The liver, positioned between the intestine which absorbs nutrients and other organs which utilize nutrients, holds an extraordinary position in the metabolism of ingested nutrients. Blood is supplied via the portal vein (about 80% of flow) and the hepatic artery (about 20% of flow), the liver drains its metabolites into the bile system or inferior vena cava. Within the liver, the hepatocytes form a trabecular network, facing the sinusoids with their basolateral surface and forming the bile canaliculi with their apical membranes. In the hepatobiliary system, metabolites, such as fatty acid or drugs, are metabolized and excreted by hepatocytes into the bile system. Relatively little is known about the heterogeneity of hepatocytes in relation to the bile system. Therefore, clarification of the metabolic and functional potential among cells within different compartments of the liver is of significant interest in hepatology [1–3].

The heterogeneity of hepatocytes is linked closely to the position of the cell within the liver, which in turn is related to the blood supply. Among different nomenclatures proposed to describe liver's smallest units [4], classical lobule takes the form of hexagonal prism with a branch of hepatic vein called central vein running along the central axis and surrounded by portal triads of portal veins, hepatic arteries and bile ducts at the corner [5]. Liver acinus is however delineated according to the blood flow pattern from the portal tract to the central vein. And it is organized into three zones with Zone 1 adjacent to the portal tract, and Zone 3 being closest to the central vein. Zone 2 is described as the less well-defined region between Zones 1 and 3 [6]. Caused by factors such as oxygen concentration gradient, the hepatocytes within acinus are heterogeneous with respect to their composition of cellular organelles [7],

Biomedical Optics EXPRESS

enzymes [2,8,9], receptors, transporters [10,11], regulators [12], and transcription factors [13].

Liver perfusion and *in vivo* studies have shown that different regions of the liver clear fluorescent probe molecules at different rates [11,14]. Specifically, studies on organic anions show that the probe molecule 6-carboxyfluorescein diacetate (6-CFDA) is transported from the sinusoid to hepatocyte at the basolateral membrane by multidrug resistance protein 1 (MRP1) [15] or organic anion transporting polypeotides (OATPs) [16,17]. Upon hepatocyte uptake, 6-CFDA is hydrolyzed into fluorescent 6-carboxyfluorescein (6-CF) (6-CF, Fig. 6, Appendix 1) by intracellular nonspecific esterase with emission at 517 nm [18–20] and subsequently excreted into the bile canaculi via ATP-binding cassette (ABC) transport proteins on hepatocyte apical membrane [21]. However, metabolic kinetics at the single hepatocyte level remains to be unclear.

In this study, we investigated acinar heterogeneity in hepatobiliary metabolism at single hepatocyte level, using the probe 6-CFDA as model compound. In our approach, we acquired time-lapse, two-photon imaging to investigate the hepatobiliary metabolism at single hepatocyte level across hepatic acinus, as the concentration of the fluorescent 6-CF changed with time. Moreover, kinetic constants characterizing hepatobiliary metabolism was achieved at single pixel resolution. Image-based kinetic analysis of 6-CFDA metabolism allows direct visualization of functional heterogeneities among hepatocytes.

2. Experimental methods and systems

2.1 Two-photon fluorescence microscopy

The two-photon fluorescence microscopy used in this study was a modified version of a home-built laser scanning microscopic system based on an inverted microscope (Nikon TE-2000, Tokyo, Japan). The excitation source was a titanium-sapphire laser with 780 nm output (Tsunami, Spectra-Physics, Mountain View, CA) pumped by a diode-pumped solid-state laser (Millennia X, Spectra-Physics). The laser beam was scanned in a focal plane by an x-y mirror scanning system (model 6220, Cambridge Technology, Bedford, MA), and then guided toward the inverted microscope. An objective (20X, PlanFluor oil immersion, numerical aperture 0.75, Nikon, Japan) was used to focus the laser beam into the sample. The emission, collected in a epi-illuminated geometry was separated into four simultaneous detection channels by serial dichroic mirrors (435DCXR, 495DCXR, 555DCLP, Chroma Technology, Rockingham, VT) (Fig. 7(B), Appendix 2) as well as by additional band-pass filters (HQ390/20, HQ460/50, HQ525/50, HQ610/75, Chroma Technology) [20]. For each optical scan was composed of 512 × 512 pixels (180 × 180 μm^2) by Nikon 20X objective, resulting in the acquisition of a total of 3 × 3 frames scanned in one minute to compose an image (1536 × 1536 pixels, 540 × 540 μm^2).

2.2 Wide-field fluorescence microscopy

The wide-field fluorescence microscopy, of which the excitation source was an Argon laser with 514 nm output, was employed in the study. Its optical path followed that of the two-photon fluorescence microscopy, except having the x-y mirror system fixed. Moreover, the same objective, through which the laser beam was dispersed, was adopted with an additional lens. The collected emission was passed through the dichroic mirror (525DCLP, Chroma Technology, Rockingham, VT) and the band-pass filter (HQ590/80, Chroma Technology, Rockingham, VT). For fluorescence imaging acquisition, high sensitivity EM-CCD (iXon DV887DCS-BV, Andor Technology, Ireland) was utilized. (Fig. 7(A), Appendix 2).

2.3 Experiment animals

Wild type male C57BL/6 mice (23 ± 2 g) at the age of seven to eight weeks were purchased from the Laboratory Animal Center of the National Taiwan University Hospital and kept in a

Biomedical Optics EXPRESS

12 hrs light/ 12 hrs dark cycle under a regulated environment (23 ± 1 °C). The mice were housed in plastic cages with free access to food and water. All procedures followed the guidelines for humane treatment of animals set by the Laboratory Animal Center of the National Taiwan University Hospital.

2.4 Installation of metallic liver window device (window and stage)

Experimental mouse was first anesthetized by intraperitoneal injection (IP injection) of 2-2-2 tribromoethanol (0.35 mg/g body weight) and laparotomy was performed for the installation of hepatic imaging window on the liver surface [19,20]. The liver surface under the window was thus circumscribed for image acquisition using two-photon fluorescence microscopy. Prior to the fluorescence injection, the window attached the mouse was fixed onto a square plate [19]. The plate was subsequently put onto the stage of the microscope. To prolong the anesthesia period and keep the mouse in deep anesthetic status, gas anesthetic (isoflurane, Forane, Abbott Lab. Ltd, England, 0.5%-500cm^3/min) was used.

The depth of hepatic imaging was about 30 μm below liver surface. For hepatic imaging acquisition, wide field (Fig. 7(A), Appendix 2) and two-photon fluorescence microscopies (Fig. 7(B), Appendix 2) were employed for delineating the acinus for imaging and examining the metabolism of 6-CFDA molecular probe in hepatocytes.

2.5. Fluorescence chemistry

Rhodamine B isothiocyanate-dextran (RITC-dextran, MW~70,000 da on average, Sigma Chemical, St, Louis, Mo, USA) and 6-carboxyfluorescein diacetate (6-CFDA) (1mg/ml, Sigma Chemical, USA) were injected intravenously into the mice for vessel labeling and hepatobiliary function imaging, respectively. RITC-dextran solute concentration was 50 mg/ml, and the main emission of RITC-dextran was at 590 ± 40 nm. As for 6-CFDA, 6-carboxyfluorescein (6-CF) and 2 acetate ($CH_3CO_2^-$) were the two reaction products after the hydroxylation of 6-CFDA by intracellular esterases [18] (Fig. 6, Appendix 1). Acetate was a non-fluorescent organic molecule and 6-CF was a fluorescent organic molecules. The emission range of 6-CF was around 517 nm.

2.6 Blood flow direction

Rhodamine B isothicyanate (RITC)-dextran 70,000 (2.50 mg/mouse, Sigma, Saint Louis, MO) was intravenously injected via the catheter to visualize blood vessels of anesthetized mouse [19,20]. For the preparation of intravenous fluorescence injection, a catheter (PE-10, BD (Becton Dickinson and Company), NJ, USA) was inserted into the jugular vein of the anesthetized mouse. From there, RITC-dextran would perfuse to hepatic portal tract consisting of hepatic artery, hepatic portal vein and bile duct.

The fluorescence signal of RITC-dextran at the bandwidth range of 550-630 nm was recorded and assigned to the red pseudocolor to elucidate the dark RBCs within the sinusoid. By tracking the dark RBCs, time-lapse images at 0.10-sec intervals allowed us to visualize the direction of blood flowing from portal tracts to central veins. Sinusoids could be resolved and tracked to depths of up to 30 μm under the liver surface.

2.7 Imaging process

The fluorescence signals of RITC-dextran and 6-CF were merged by IDL 6.3 (EXELI Visual Information Solution, USA) software for hepatobiliary imaging. By fitting, IDL 6.3 code with the mathematical function of 6-CF intensity, the metabolic rates of 6-CFDA from vessels to hepatocytes (k_1) and of 6-CF form hepatocytes to bile canaliculi were plotted to k_2-distribution for ImageJ analysis.

Biomedical Optics EXPRESS

3. Results

3.1 Identification of a functional microcirculation liver unit, acinus

To identify a functional microcirculation liver unit, acinus, in living mouse liver, we modified the method of plasma labeling descried by Varghese et al. [22] using inverted wide-field fluorescence microscopy (Fig. 7(A), Appendix 2). After injecting anesthetized mice with rhodamine B isothiocyanate (RITC)-dextran through jugular vein, we tracked the motion of nonfluorescent erythrocytes using time-lapse video microscopy and visualized direction of blood flow from portal tracts to central veins (Fig. 8, Appendix 3), thereby identifying the locations of the portal and central veins (Fig. 1) for defining hepatic acinus and its relative position to hexagonal lobules.

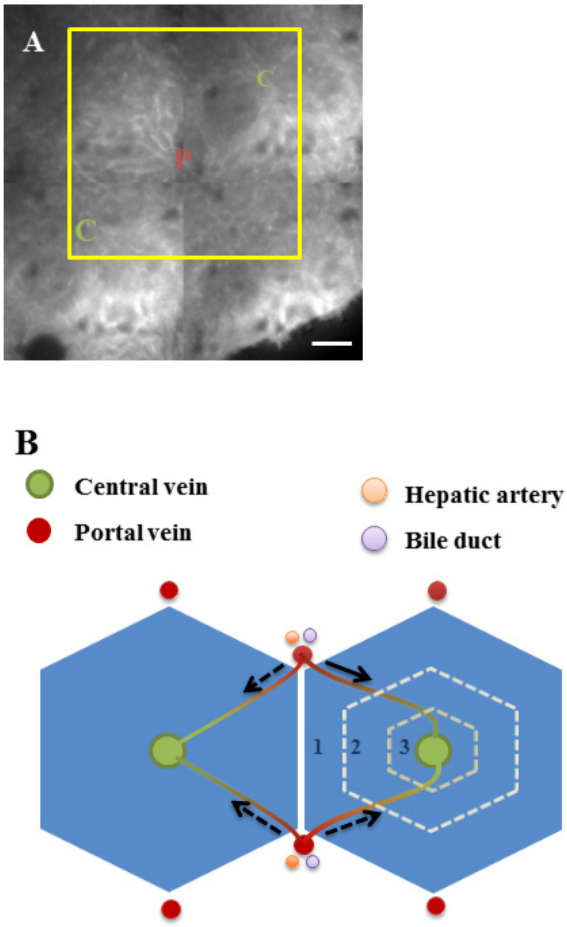

Fig. 1. (A) Identification of hepatic acinus in mouse liver by intravital wide-field fluorescence imaging C and P denote central and portal regions, respectively. The square region containing the acinus is the image field of two-photon fluorescence microscopy for observing 6-CFDA metabolism (Scale bar: 100 μm). (**B**) Depiction of blood flow in the hepatobiliary system where hepatocytes are assigned arbitrarily to 3 groups (Zones 1, 2, and 3).

3.2 Examination of 6-CFDA metabolism

Following identification of the acinus, we injected the mice with 6-CFDA through jugular vein, and used time-lapse, two-photon fluorescence microscopy for imaging (Fig. 7(B), Appendix 2). 6-CFDA metabolism within the acinus was then examined as processed 6-CF

Biomedical Optics EXPRESS

molecules are excreted into the bile canaliculi through transporters such as multidrug resistance protein 2 (MRP2) (Fig. 2(A)-2(F)). For each pixel, time-lapse 6-CF fluorescence was plotted (Fig. 2(G)).

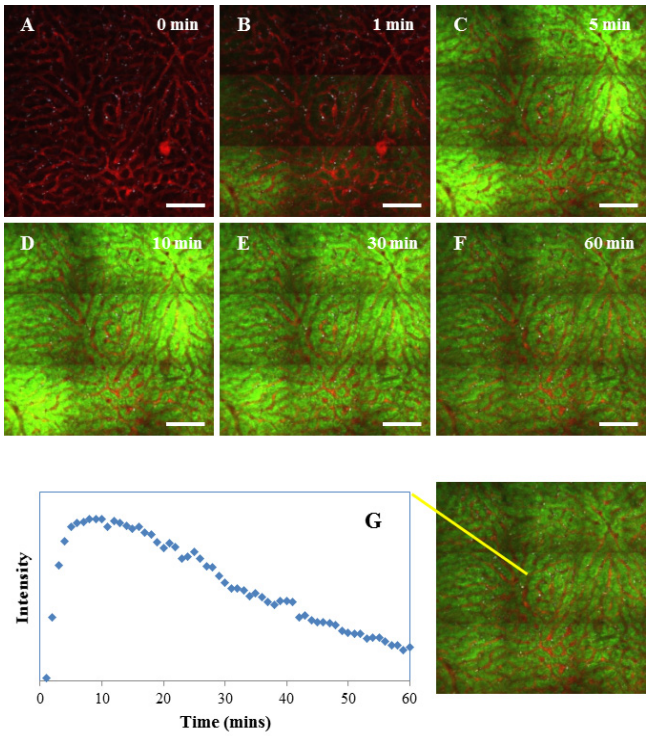

Fig. 2. Dynamic hepatocellular metabolism of 6-CFDA. 6-CFDA is uptaken from sinusoids into hepatocytes, where intracellular esterase metabolizes the molecule into 6-CF (fluorescent) and acetate and the resultant 6-CF is subsequently excreted through bile canaliculi. (**A**)~(**F**) are time-lapse images of 6-CFDA metabolism at 0, 1 min, 5 mins, 10 mins, 30 mins, and 60 mins. Red is rhodamine B-dextran (RITC), green represents 6-CF fluorescence, and white is hepatic stellate cell (Scale bar: 100 μm). (G) Illustration of the extraction of 6-CF fluorescein profile from a single pixel.

3.3 Quantification of 6-CFDA metabolic rate in hepatocytes

To quantify the metabolic rate of 6-CFDA in hepatocytes, a first-order, kinetic model was used to describe the kinetics of 6-CF fluorescence within the hepatocytes. Specifically, the concentrations of 6-CFDA in the sinusoid and 6-CF in the hepatocyte can be described by Eqs. (1) and (2) respectively as

$$\frac{d\left[6-CFDA\right]_s}{dt} = -k_1\left[6-CFDA\right]_s \tag{1}$$

$$\frac{d\left[6-CF\right]_H}{dt} = k_1\frac{V_B}{V_H}\left[6-CFDA\right]_s - k_2\left[6-CF\right]_H \tag{2}$$

where $\left[6-CFDA\right]_s$ is sinusoidal concentration of 6-CFDA and $\left[6-CF\right]_H$ is 6-CF concentration of the hepatocyte. In this model, k_1 and k_2 are the respective metabolic rate constants for hepatocyte uptake/processing and excretion into the bile canaliculi. Finally, V_B

Biomedical Optics EXPRESS

is the blood volume and V_H is the volume of hepatocyte. The ratio V_B / V_H in Eq. (2) accounts for difference in volume between the sinusoid and hepatocyte. These equations can be solved to derive concentrations of 6-CFDA in the sinusoid and 6-CF and the hepatocytes:

$$\left[6-CFDA\right]_s = \left[6-CFDA\right]_0 e^{-k_1 t} \tag{3}$$

$$\left[6-CF\right]_H = \frac{k_1}{k_1 - k_2}\left[6-CFDA\right]_0 \frac{V_B}{V_H}\left(e^{-k_2 t} - e^{-k_1 t}\right) \tag{4}$$

with $\left[6-CFDA\right]_0$ as the initial 6-CFDA concentration in the sinusoid.

In quantifying the metabolic rate of 6-CFDA, Eq. (4) was used for fitting the 6-CF fluorescence intensity profile at each pixel of the time-lapse images (Fig. 3). Furthermore, images of the sinusoid and hepatic stellate cells, labeled by RITC-dextran and autofluorescence respectively, were used as masks. In this manner, spatial distributions of the metabolic rate constants k_1 and k_2 of the hepatic cords can be highlighted (Fig. 4(A) and 4(B)). These images show that the spatial distributions of the kinetic rate constants are heterogeneous, with a gradient of increasing metabolic rate from portal (Zone 1) to central regions (Zone 3). Moreover, by plotting the metabolic rate constants from portal to central region, the gradient for k_2 can be seen to be higher than that of k_1 (Fig. 9, Appendix 4 and Fig. 10, Appendix 5). In addition, the metabolic constants between two adjacent hepatocytes vary significantly and are not continuous.

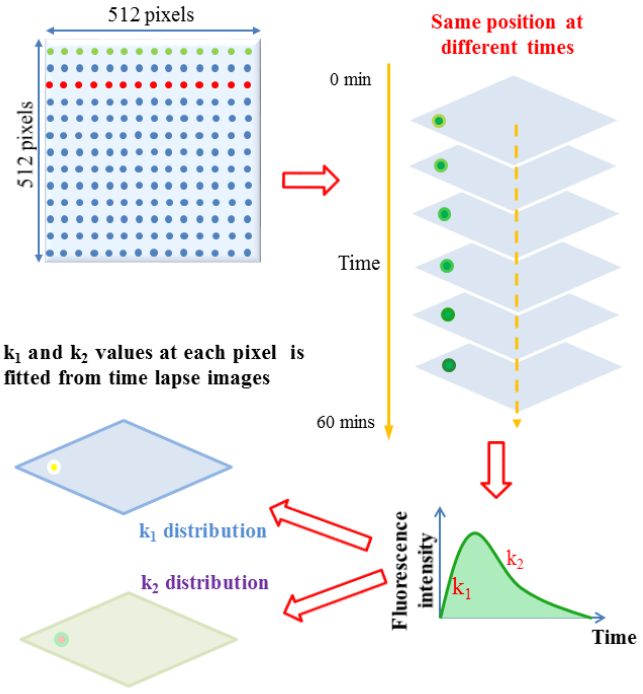

Fig. 3. Fitting of metabolic rate constants with single pixel resolution. Temporal profile of 6-CF fluorescence at each pixel is fitted to the kinetic model to yield image maps of kinetic rate constants.

Biomedical Optics EXPRESS

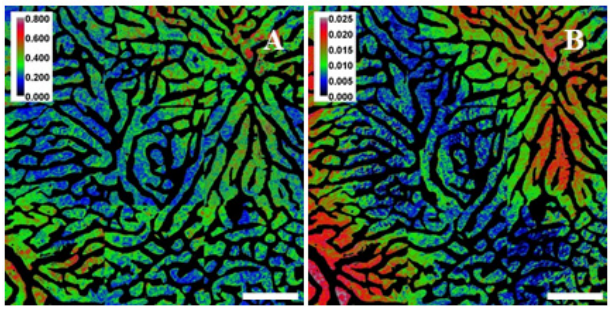

Fig. 4. (A) The spatial distribution of k_1 values after the first-order mathematical fitting, (B) The distribution of k_2 values after the first-order mathematical fitting.

3.4 Definition of zonation by color distribution of k_2-value

In the periportal area, the hepatobiliary excretory rate of 6-CF is smaller than that in the pericentral area (Fig. 4(B)). In between these two areas, the middle area exhibits a gradient from pericentral to periportal areas. In our results, the metabolic constants can be used to distinguish different regions of metabolic potentials. We used the color distribution of k_2-value to distinguish different zones. We defined the blue, green and red regions of k_2-distribution to be Zones 1, 2, and 3 for kinetic constant analysis (Fig. 5(A)). Zones 1, 2 and 3 were defined by spatial contributions and k_2 coefficient contribution. In this manner, the three zones defined are divided approximately into three regions with similar spacing.

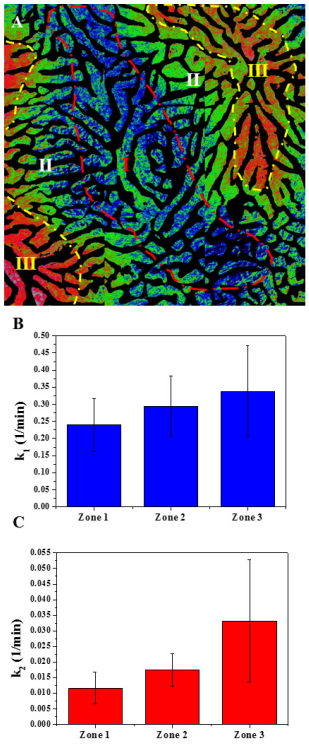

Fig. 5. k_2-value distribution analysis. (A) The k_2-result of a representative image is used to delineate Zones 1, 2, and 3. (B) The averages of k_1 values and (C) averages of k_2 values in three zones (10 hepatocytes in each zone) and total number of mice is 5.

Biomedical Optics EXPRESS

3.5 Analysis of k_1 and k_2 values

In each mouse, we chose 10 random hepatocytes in each defined Zones 1, 2, and 3, to analyze the sinusoidal uptake coefficient k_1 and apical excreting coefficient k_2. The k_1 distribution displays a gradient similar to that of the k_2 results. For the five mice used, the sinusoidal uptake coefficients k_1 of Zones 1, 2, and 3 were respectively 0.239 ± 0.077, 0.295 ± 0.087, and 0.338 ± 0.133 min^{-1}, the apical excreting coefficients k_2 of Zones 1, 2, and 3 were 0.0117 ± 0.0052, 0.0175 ± 0.0052, and 0.0332 ± 0.0195 min^{-1}, respectively. These results presented that hepatocytes in Zone 3 play the major role of 6-CFDA metabolism in liver *in vivo*. For sinusoidal uptake, the k_1 value of Zone 3 was 41.4% higher than that of Zone 1. The k_2 value of Zone 3 was 183.8% higher than that of Zone 1 (Fig. 5(B) and 5(C)). The metabolic efficiency defined to be k_2/k_1 of Zone 3 was 2.01 times higher than that of Zone 1 (Table 1).

Table 1. Zonal metabolic coefficients

	Zone 1	Zone 2	Zone 3
k_1 (min^{-1})	0.239 ± 0.077	0.295 ± 0.087	0.338 ± 0.133
k_2 (min^{-1})	0.0117 ± 0.0052	0.0175 ± 0.0052	0.0332 ± 0.0195
k_2/k_1	0.0490	0.0593	0.0982

4. Conclusion

This work determines the spatial distribution of the functional heterogeneities. Our results show the fact that Zone 3 is the main area of hepatic acinus in performing hepatobiliary metabolism. k1 and k2 values of pericentral area are both greater than periportal area. Our image analysis results correspond with the hepatic acinar structure in functional definition. Here, hepatocytes are non-uniform in their positions and cellular functions. This approach can be used for drug testing and analyzing the effect of hepatic metabolism with age [23] and metabolic diseases *in vivo*. Our methodlogy may provide additional information in understanding hepatobiliary zonal metabolism when in mouse models of different pathological conditions, and provide valuable insights in clinical medicine.

Appendix 1

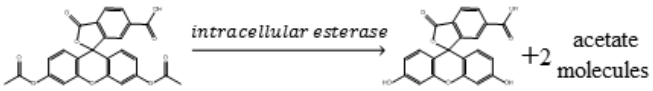

Fig. 6. Function of 6-carbroxyfluorescein diacetate intracellular esterase.

Biomedical Optics EXPRESS

Appendix 2

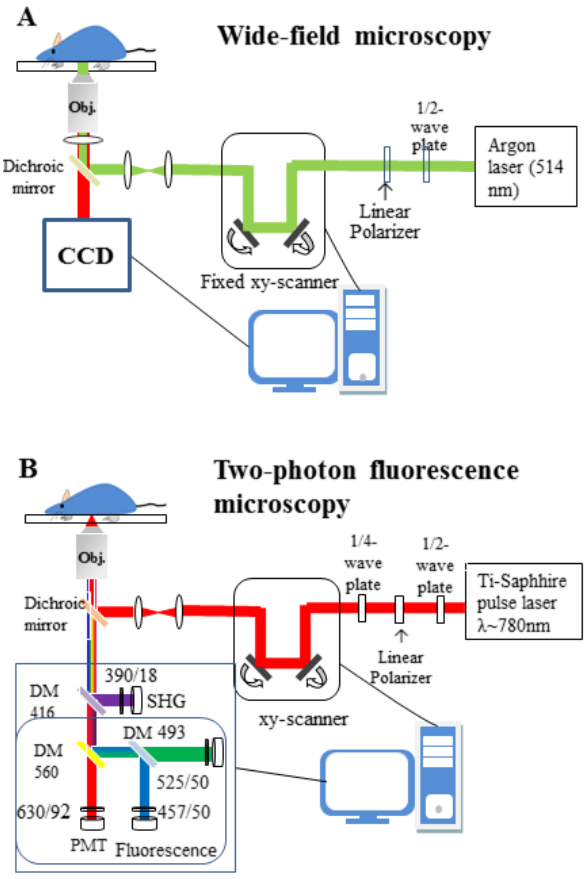

Fig. 7. Optical setup of experiments. (**A**) Wide-field fluorescence microscopy and (**B**) two-photon fluorescence microscopy.

Appendix 3

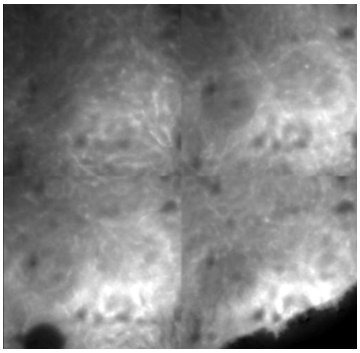

Fig. 8. Movie (see Visualization 1).

Biomedical Optics EXPRESS

Appendix 4

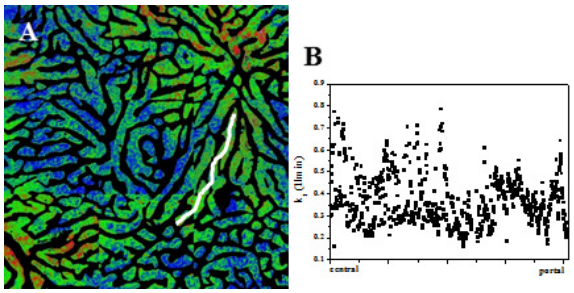

Fig. 9. k_1 values display minor gradient in portal-central axis. (A) Take a line from Zone 1 to Zone 3 in the k_1-result. Scale bar is 100μm. (B) The k_1-value plot of the portal-central axis.

Appendix 5

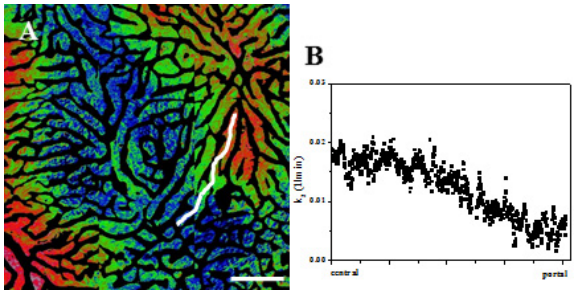

Fig. 10. k_2 values showing a gradient in portal-central axis. (A) Take a line from Zone 1 to Zone 3 in the k_2-result. Scale bar is 100 μm. (B) The k_2-value plot of the portal-central axis.

Acknowledgments

We acknowledge the support of grants from the Ministry of Science and Technology (National Science Council) (NSC101-2112-M-002-003-MY3, NSC102-2221-E-002-030-MY3) in Taiwan, National Taiwan University (NTU103R7804), the Center for Quantum Science and Engineering (NTU-ERP-103R891401).